# Spectral Diffusion and Electron-Phonon Coupling of the B800 BChl *a* Molecules in LH2 Complexes from Three Different Species of Purple Bacteria

J. Baier,[†] M. Gabrielsen,[‡] S. Oellerich,[†] H. Michel,[§] M. van Heel,[¶] R. J. Cogdell,[‖] and J. Köhler[†]*

[†]Experimental Physics IV and Research Centre for Bio-Macromolecules, University of Bayreuth, Bayreuth, Germany; [‡]Division of Infection and Immunity, Faculty of Biomedical and Life Sciences, Biomedical Research Building, University of Glasgow, Glasgow, United Kingdom; [§]Department of Molecular Membrane Biology, Max-Planck Institute of Biophysics, Frankfurt, Germany; [¶]Department of Biological Sciences, Imperial College London, London, United Kingdom; and [‖]Division of Molecular and Cellular Biology, Faculty of Biomedical and Life Sciences, Biomedical Research Building, University of Glasgow, Glasgow, United Kingdom

ABSTRACT We have investigated the spectral diffusion and the electron-phonon coupling of B800 bacteriochlorophyll *a* molecules in the peripheral light-harvesting complex LH2 for three different species of purple bacteria, *Rhodobacter sphaeroides*, *Rhodospirillum molischianum*, and *Rhodopseudomonas acidophila*. We come to the conclusion that B800 binding pockets for *Rhodobacter sphaeroides* and *Rhodopseudomonas acidophila* are rather similar with respect to the polarity of the protein environment but that the packaging of the $\alpha\beta$-polypeptides seems to be less tight in *Rb. sphaeroides* with respect to the other two species.

## INTRODUCTION

Proteins represent a class of materials whose function is directly connected to structural fluctuations. Although many proteins show well-resolved x-ray diffraction patterns their structure is not unique. To fulfill their biological functions, proteins are quite flexible and exist in a variety of conformations (1). Transitions between these conformations give rise to rich dynamics, which is commonly modeled by a rugged energy landscape, i.e., a complicated potential energy surface with a large number of minima, saddle points, and a broad distribution of barriers (2,3). Chromophores that are embedded in the protein will sense rearrangements in the protein as a change in the distance-dependent interactions in their local environment and react sensitively to these fluctuations by changes of their electronic spectra (4–7). Briefly, the transition between the electronic ground state and the electronically excited state of a chromophore gives rise to a homogeneously broadened zero-phonon line (ZPL). However, the electronic excitation of the molecule corresponds to a change of its wave functions and can be accompanied by a change of the equilibrium positions of its constituting atoms. Hence, if the molecule is embedded in a matrix, for example a protein, the electronic excitation can induce low-frequency vibrations in the local environment of the molecule. As a result of this, the ZPL is accompanied by a relatively broad phonon side band (PSB) that represents an electronic transition in combination with the simultaneous excitation of low-frequency vibrations of the host. For convenience we will refer to these intermolecular vibrations as phonons, independent of the crystallinity of the host system. These should not be confused with the intramolecular vibrations that occur at higher energies (8) and that give rise to vibronic coupling.

The profile of the electronic spectrum, i.e., the distribution of the intensity between the ZPL and the PSB, is determined by the linear electron-phonon coupling strength (9). Information about the interaction between the chromophore and the protein matrix is provided by both the spectral position of the ZPL and the ratio of the integrated intensity between the ZPL and the PSB (10). The spectral position of the ZPL, on the one hand, is fine-tuned by the distant-dependent interactions in the vicinity of the chromophore, which provides a sensitive tool to monitor fluctuations in the interactions between the chromophore and the protein matrix via the spectral fluctuations (spectral diffusion) of the chromophore (11). On the other hand, the integrated intensity of the PSB is associated with the displacement of the equilibrium positions of the nuclei on a photoexcitation of the chromophore. In other words, the matrix-induced shift of the ZPL and the relative intensity of the PSB are related to the vertical and horizontal displacements of the potential energy curves in the two electronic states of the chromophore, respectively (12).

In recent years, numerous high-resolution spectroscopic studies were devoted to study spectral diffusion processes in proteins (13–16). In hole-burning experiments such spectral fluctuations show up as waiting-time dependent line broadening of the optical transition, whereas in single-molecule experiments these spectral fluctuations can be directly observed as spectral trails (17). As yet, less attention has been spent on monitoring the electron-phonon coupling of chromophores in proteins by single-molecule spectroscopy. The reason for this is that the protein undergoes structural fluctuations that give rise to spectral fluctuations of the chromophore. If these fluctuations occur on a much faster timescale than the temporal resolution of the experiment, only

*Submitted May 4, 2009, and accepted for publication July 14, 2009.*

*Correspondence: juergen.koehler@uni-bayreuth.de

Editor: Janos K. Lanyi.



0006-3495/09/11/2604/9 $2.00

doi: 10.1016/j.bpj.2009.07.052

the temporal average of the spectrum is observed with a concomitant loss of spectral information (18). We have shown recently that temporal averaging can be reduced tremendously by exploiting pattern recognition techniques for data analysis (19,20).

In this study, we compare both the spectral diffusion and the linear electron-phonon coupling of bacteriochlorophyll (BChl) *a* molecules that are naturally embedded in the peripheral light-harvesting complex 2 (LH2) from three species of photosynthetic purple bacteria: *Rhodopseudomonas acidophila, Rhodospirillum molischianum*, and *Rhodobacter sphaeroides* strain 2.4.1. Owing to the BChl *a* molecules, the LH2 complexes are auto-fluorescent and can be studied noninvasively. For the aforementioned species, the structures of the LH2 complexes were determined by x-ray crystallography (*Rps. acidophila* and *Rsp. molischianum*) (21,22) or electron-microscopy (*Rb. sphaeroides* strain 2.4.1) (23). Remarkably, these peripheral light-harvesting complexes form circular oligomers of the basic building block that is a protein heterodimer ($\alpha\beta$), which binds three BChl *a* pigments and one carotenoid molecule. The total LH2 complex consists either of nine (*Rps. acidophila, Rb. sphaeroides*) or eight (*Rsp. molischianum*) such $\alpha\beta$-polypeptide heterodimers, where the chromophores are arranged in two concentric rings called B800 and B850, according to their room-temperature absorption maxima. The B850 ring consists of 18 (16 for *Rsp. molischianum*) strongly excitonically coupled BChl *a* molecules, whereas the B800 ring is formed by nine (eight for *Rsp. molischianum*) well-separated BChl *a* molecules, which are suited to act as sensitive probes to monitor conformational changes in their local environment (24,25).

Commonly, spectral diffusion experiments are carried out at cryogenic temperatures. The advantages of working at low temperatures are i), negligible photobleaching, which enables long observation times and concomitantly an improvement of the signal/noise ratio of the spectra; ii), a tremendous reduction in the linewidths of the spectral features due to the suppression of thermal motions of the nuclei, which allows the resolution of narrow spectral features that even for a single molecule would be hopelessly broadened at room temperature; and iii), a shift of the rates of the conformational changes to timescales where those structural fluctuations become experimentally accessible. However, a serious issue that is often raised is that the results of those experiments, far from physiological conditions, might be irrelevant for our understanding of the functioning of proteins. The idea of our approach is that conformational changes of the protein can be induced by optical excitation of the pigments and subsequent relaxation of the excited state (26). The photon energy of ~12,500 $cm^{-1}$ for the B800 absorptions that is dissipated this way exceeds by far the thermal energy at 1.4 K at which the optical experiments are carried out. Given the low fluorescence quantum yield of LH2 of ~10% (27) a large fraction of the average absorbed energy is dissipated by radiationless decay and involves a momentary excitation of nuclear motion. On relaxation back to thermal equilibrium there is a finite probability that the system ends up in a different conformational substate, which will be manifested by a change in transition energy of the chromophore. Therefore the space of conformational substates that is probed by the induced structural fluctuations is not restricted to the part of the energy landscape that is accessible under thermal equilibrium, i.e., the range of the subset of displacements is not determined by the low temperature. Hence, working at cryogenic temperatures offers an ideal opportunity to study the organization of the protein energy landscape in great detail.

In previous works we studied the spectral dynamics of the B800 BChl *a* molecules in individual LH2 complexes from *Rb. sphaeroides* (28,29) and *Rsp. molischianum* (6,7,30). We followed the spectral trails of individual absorptions as a function of time and determined the statistics of the changes in spectral positions. For the latter species, occasional spectral jumps in the order of several hundred wavenumbers were observed. To our surprise the spectral changes in the B800 band from *Rb. sphaeroides* did not show these large spectral variations. It is very intriguing that the spectral diffusion behavior of LH2 complexes from *Rsp. molischianum* and *Rb. sphaeroides* seems to differ so markedly. Unfortunately, at the moment there is no high-resolution structure available for LH2 complexes from *Rb. sphaeroides* and it is not possible to compare the immediate chromophore environment for the two species directly. To shed more light on this issue we compare the spectral diffusion behavior and the electron-phonon coupling strength of LH2 for the bacterial species *Rsp. molischianum* and *Rps. acidophila* for which high-resolution x-ray structures are available (21,22) with that of *Rb. sphaeroides* strain 2.4.1 for which only a lower resolution electron density map exists (23).

## MATERIALS AND METHODS

The LH2 complexes were isolated and purified as described previously (31) and the resulting solution was diluted in several steps to a concentration of ~$10^{-11}$ M. Dilution was carried out in detergent buffer to prevent the complexes from aggregation or dissociation; in the last step also 1.8% (wt/wt) polyvinyl alcohol (PVA; $M_w$ 125,000 g/mol) was present; 10 $\mu$l of this solution was spin-coated on a lithium fluoride substrate, producing high-quality amorphous polymer films with a thickness of $<1$ $\mu$m in which the pigment-protein complexes were embedded. For reference experiments, LH2 complexes from *Rps. acidophila* were reconstituted into a DOPC lipid bilayer as described in detail in Richter et al. (32).

After cooling the samples to 1.4 K in a liquid-helium cryostat the fluorescence-excitation spectrum of an individual light-harvesting complex was obtained in two steps. First, a $40 \times 40$ $\mu m^2$ wide-field image of the sample was taken by exciting a large area of the sample at an excitation wavelength, which coincides with an absorption maximum of the complexes (800 nm), collecting the fluorescence by an objective ($f = 3.1$ mm, NA = 0.85 used for *Rsp. molischianum* and *Rb. sphaeroides*; $f = 2.9$ mm, NA = 0.5 for *Rps. acidophila* for both matrices) mounted inside the cryostat immersed in liquid helium and focused onto a back-illuminated CCD camera (512 SB, Princeton Instruments, Trenton, NJ) after passing suitable bandpass

filters. In the next step, a spatially well-isolated complex was selected from the wide-field image and a fluorescence-excitation spectrum of this complex was obtained by only illuminating the selected complex and confocally collecting its fluorescence with a single-photon counting avalanche photodiode (APD) (SPCM-AQR-16, EG&G). Instead of obtaining a spectrum by slowly scanning the laser once, spectra were recorded in rapid succession by scanning repetitively through the spectral range of interest and storing the different traces separately. Thereby, light-induced fluctuations of the fluorescence intensity on a timescale of seconds could be diminished and information about the spectral dynamics could be obtained. With a scan speed of the laser of 44 $cm^{-1}$/s and an acquisition time of 10 ms per data point, this yields a nominal resolution of 0.44 $cm^{-1}$ ensuring that the spectral resolution is limited by the spectral bandwidth of the laser (1 $cm^{-1}$). The confocal-detection mode features a superior background suppression, which allowed fluorescence-excitation spectra to be recorded with high signal/noise ratios (33).

## RESULTS

### Spectral diffusion

In Fig. 1 *A* we show a sequence of 800 fluorescence-excitation spectra from an absorption line in the B800 band of a single LH2 complex from *Rb. sphaeroides*. The horizontal axis corresponds to the excitation energy, the vertical axis to time, and the fluorescence intensity is given by the gray scale. Fig. 1 *B* displays the spectrum that results when all 800 individual spectra are averaged. The sequential data acquisition scheme allows us to extract the relative change in spectral position as a function of time and to map out the spectral diffusion that occurs on timescales slower than the time that is required to record an individual fluorescence-excitation spectrum. The statistics of these spectral changes within the B800 band of LH2 has been determined for *Rb. sphaeroides* (15 absorptions), *Rsp. molischianum* (11), and *Rps. acidophila* (17) all solubilized in detergent and immobilized in polyvinyl alcohol (PVA). For reference purposes we have studied also LH2 complexes from *Rps. acidophila* (five absorptions) that were reconstituted into a DOPC lipid bilayer. To determine the spectral positions of the absorptions in the individual scans with high accuracy, each line has been fitted by a Lorentzian. From these data we determined the distributions of the relative change in spectral position between two successive scans. Examples for these distributions are shown in Fig. 2 from top to bottom for *Rb. sphaeroides*, *Rsp. molischianum*, *Rps. acidophila* (all in PVA), and *Rps. acidophila* (in DOPC), respectively. For better comparison, the scales of the histograms have been normalized to the total number of recorded spectra and are displayed in relative units. For example, for *Rb. sphaeroides*, 37% of the observed spectral changes occur between 0–1 $cm^{-1}$, 25% of the spectral changes occur between 1–2 $cm^{-1}$, ~1.25% of the spectral changes occur between 10–15 $cm^{-1}$, etc. Significant differences between the histograms for the detergent-solubilized and the reconstituted samples from *Rps. acidophila* are not observed, which excludes the possibility that artifacts are induced by the PVA matrix.

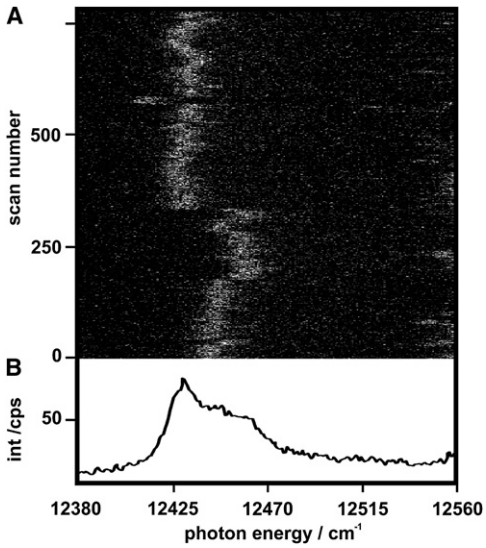


FIGURE 1 (*A*) Two-dimensional representation of 800 consecutively recorded fluorescence-excitation spectra from a part of the B800 band of an individual LH2 complex from *Rb. sphaeroides* at 1.4 K. The horizontal axis corresponds to the excitation energy, the vertical axis to the time and scan number, respectively, and the fluorescence intensity is given by the gray scale. The spectra were recorded with an excitation intensity of 10 $W/cm^2$. (*B*) Average over all fluorescence-excitation spectra in the stack. The intensity is given in counts per second (cps).

We group the observed spectral fluctuations into three categories according to the magnitude of the spectral change between two successive scans. The first category corresponds to a relative change of the absorption frequency of $<10$ $cm^{-1}$ and comprises >90% of the spectral diffusion events (Fig. 2, *first column*). Characterizing these histograms by their widths at half the maximum yields 2.1 $cm^{-1}$, 6.1 $cm^{-1}$, 4.2 $cm^{-1}$, and 3.5 $cm^{-1}$ for *Rb. sphaeroides*, *Rsp. molischianum*, *Rps. acidophila* all in PVA, and *Rps. acidophila* in DOPC, respectively. These figures, and visual inspection of Fig. 2, already suggest that the width of the distribution for *Rsp. molischianum* is larger than that for the other cases. To substantiate this conjecture we evaluated the half widths of such histograms for the full data set of all chromophores studied. This showed variations of this parameter between 1.7 and 4.5 $cm^{-1}$ for LH2 from *Rb. sphaeroides* and *Rps. acidophila* (both matrices), and between 5.0 and 8.5 $cm^{-1}$ for *Rsp. molischianum*.

The second category of spectral diffusion events corresponds to changes in spectral position that are in the order of some tens of wavenumbers (Fig. 2, *second column*); ~5–10% of all processes fall into this group and no significant differences have been found between the four types of samples. Here we find on average 20–30 $cm^{-1}$ for the spectral change between two successive scans. Finally, the third category of spectral diffusion processes refers to relative changes in spectral position of ~250 $cm^{-1}$. Such spectral fluctuations have been observed exclusively for LH2 from *Rsp. molischianum* and only for a relative small fraction of the spectra studied. This finding is in agreement with a previous study on this species where a similar low frequency of large

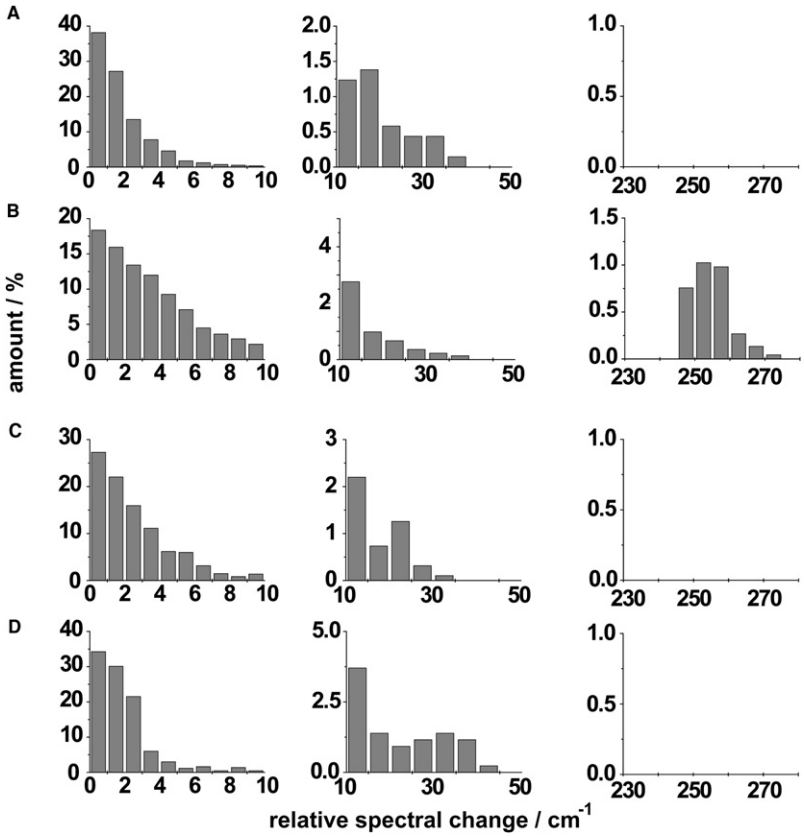


FIGURE 2 Distributions of the relative change in spectral position between two successive scans for (*A*) *Rb. sphaeroides* (in PVA), (*B*) *Rsp. molischianum* (in PVA), (*C*) *Rps. acidophila* (in PVA), and (*D*) *Rps. acidophila* (in DOPC). The scales of the histograms have been normalized to the total number of recorded spectra and are displayed in relative units.

spectral jumps has been observed. However, it is the strength of single-molecule spectroscopy to isolate such rare events that might represent key processes to obtain a basic understanding of the underlying structural fluctuations. Clearly, we cannot prove that such large spectral fluctuations never occur in *Rps. acidophila* or *Rb. sphaeroides*. Yet, our results show that the probability for the occurrence of such large spectral fluctuations in the aforementioned species must be significantly lower compared with *Rsp. molischianum*.

## Electron-phonon coupling

As a consequence of the spectral fluctuations, neither the individually recorded spectra within a stack nor the time-averaged spectra of many consecutively recorded spectra permit a quantitative analysis of the spectral profile of the electronic transition. To overcome these limitations we applied a multivariate statistical pattern recognition algorithm (MSA) (34). Such algorithms have been used for the comparison of amino acid sequences of proteins from different species or for the reconstruction of the three dimensional structure of large biological macromolecules from two-dimensional projections obtained by single particle cryo-electron microscopy (35). We have shown recently that these techniques can be applied successfully to retrieve the profiles of electronic spectra from individual objects in disordered hosts (19,20). Briefly, in the MSA analysis each individual spectrum in a stack of spectra (e.g., Fig. 1 *A*) is interpreted as a one-dimensional image. By pattern recognition techniques these spectra are grouped into a predetermined number of classes (here typically 20–100) according to their statistical similarity, such that the variance between the classes is maximized and the total intraclass variance is minimized (in a mathematical, least-squares sense). From this procedure we obtain the class-averaged spectra (CAS), that is, the average of only those individual spectra that have been assigned to the same class. In simple words, the algorithm ensures that only those individual spectra that are ''sufficiently similar'' are averaged. Further details about this algorithm can be found elsewhere (34).

The achievement of this approach is that contributions to the line broadening from spectral diffusion processes, occurring on timescales slower than the time required to scan the laser across an individual transition, are eliminated. This allows the registration of the spectra from an individual chromophore with a drastically reduced spectral linewidth without the usual trade-off between spectral and/or temporal resolution versus signal/noise ratio. Typical examples for class-averaged spectra from individual absorptions in the B800 band of LH2 from the different species are shown in Fig. 3. The spectra consist of a relatively narrow ZPL accompanied by a weak broad PSB on the high-energy side.

Within the Born-Oppenheimer approximation the electron-phonon coupling can be described by the Debye-Waller factor $\alpha$, or likewise by the Huang-Rhys factor S, defined as $\alpha = \frac{I_{\mathrm{ZPL}}}{I_{\mathrm{ZPL}} + I_{\mathrm{PSB}}} = e^{-\mathrm{S}}$ where $I_{\mathrm{ZPL}}$ ($I_{\mathrm{PSB}}$) refers to the integrated

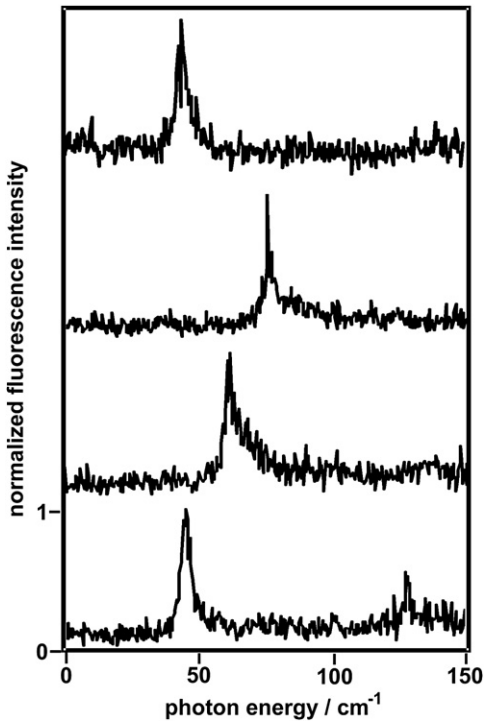


FIGURE 3 Examples of class-averaged spectra of individual absorptions in the B800 band of LH2 for, from top to bottom, *Rb. sphaeroides* (in PVA), *Rsp. molischianum* (in PVA), *Rps. acidophila* (in PVA), and *Rps. acidophila* (in DOPC). The spectra are normalized for better comparison.

intensity of the ZPL (PSB), respectively. To extract the PSB from the class-averaged spectrum we subtracted a Lorentzian from the spectral profile that was fitted to the low-energy half of the ZPL. This procedure allowed us to determine the Debye-Waller factor $\alpha$ and the mean phonon energy $\omega_m$, which is the difference in energy between the peak position of the ZPL and the spectral center of gravity of the PSB, for all absorptions studied.

The distributions of these parameters are shown in Fig. 4 for the four types of samples. Irrespective of the matrix that has been used to immobilize the LH2 complexes from *Rps. acidophila*, the distributions of the Debye-Waller factors cover the range from 0.5 to 0.7 (FWHM) and feature a peak at ~0.6. Similar figures are found for LH2 from *Rsp. molischianum*. In contrast to these findings, with LH2 from *Rb. sphaeroides* the distribution of this parameter is shifted toward smaller values and covers the range between 0.25 and 0.6 peaking at ~0.45, see Fig. 4. The histograms of the mean phonon energies, shown in Fig. 4, *right column*, feature broad distributions peaking between 20 $cm^{-1}$ and 30 $cm^{-1}$ for all four types of samples.

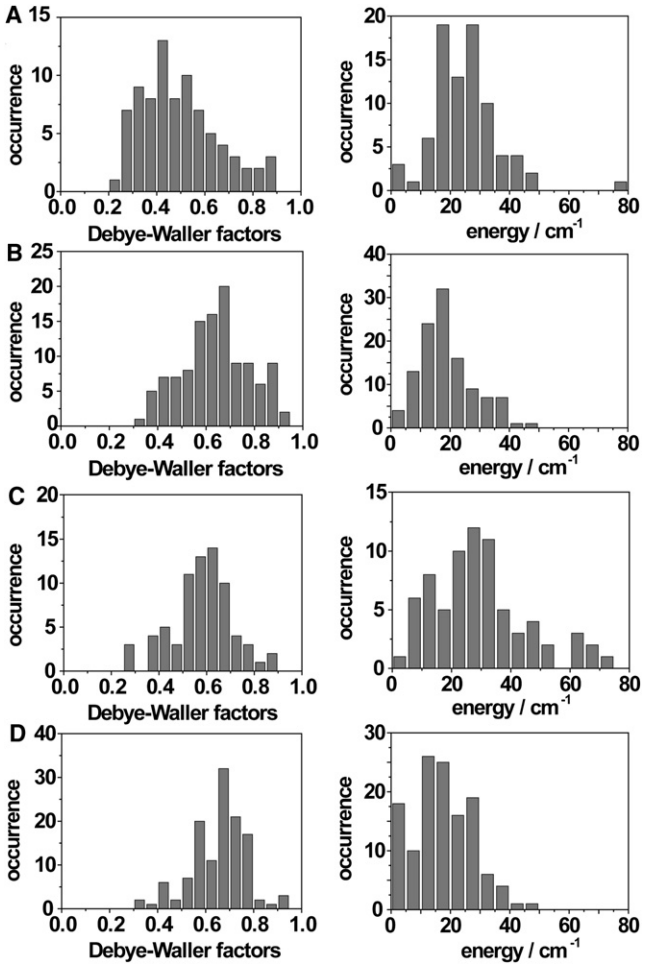


FIGURE 4 Histograms of the Debye-Waller factor (*left*) and mean phonon energies (*right*) for (*A*) *Rb. sphaeroides* (in PVA), (*B*) *Rsp. molischianum* (in PVA), (*C*) *Rps. acidophila* (in PVA), and (*D*) *Rps. acidophila* (in DOPC).

## DISCUSSION

The energies of the electronic levels of a chromophore that is embedded in a matrix are fine tuned by the electrostatic interactions with its local surroundings. For an uncharged chromophore, the main contributions to these interactions come from dipole-dipole, dipole-induced dipole, and dispersive forces, which typically fall off with $R^{-n}$, where $n$ lies between 6–12 (36). In a dynamic environment, such as a protein, the strengths of these forces are modulated by structural fluctuations of groups of atoms or molecules and as a result of this, the spectral positions of the optical transitions of the chromophore fluctuate as well, giving rise to spectral diffusion (11). Moreover, the interactions of the chromophore with the molecules in its surroundings also depend on the electronic configuration of the chromophore and change on optical excitation. This causes variations in the equilibrium positions of the nuclei that couple the electronic excitation to the nuclear motions. Within the Born-Oppenheimer approximation, the potential energy curve in the electronically excited state of the chromophore is shifted along the nuclear coordinates and features a different curvature with respect to the potential energy curve in the electronic ground state of the chromophore. This mutual displacement

of the potentials reflects the linear electron-phonon coupling, which is observable as a PSB, whereas the change in curvature leads to quadratic electron-phonon coupling, which causes a temperature dependent contribution to the homogeneous linewidth of the ZPL (10). The linear electron-phonon coupling strength is larger the larger the variations of the intermolecular interactions are on electronic excitation. These variations arise from contributions that are related to changes of the intrinsic dipole moment of the chromophore (changes of the electrostatic interactions) and from those that are related to changes of the polarizability (changes of the dispersion interactions) (10,12). Hence both phenomena, spectral diffusion and linear electron-phonon coupling, are sensitive to the variations of the intermolecular interactions in the vicinity of the chromophore. In the experiments discussed in this study, the observed low-temperature linewidths of the B800 absorptions reflect the superposition of homogenous line broadening due to fast excitation-energy transfer to the B850 manifold (37,38), and inhomogeneous line broadening due to spectral diffusion. Contributions to the homogenous linewidth from quadratic electron-phonon coupling cannot be resolved and will not be considered here.

For all three species the linear electron-phonon coupling falls into the regime of weak coupling as manifested by Debye-Waller factors (DWF) that do not fall below 0.2. Generally, this is in line with the observation that on excitation the changes in effective dipole moment for the nonpolar BChl *a* molecule of ~1 D are relatively small (39). Nevertheless, the observed DWF for the B800 BChl *a* molecules from *Rb. sphaeroides* are clearly smaller than those for the other two species. This indicates a larger change of the average distance between the nuclei in the BChl *a* molecule on electronic excitation. This finding is consistent with results from pressure-dependent hole-burning experiments (40). There it was observed that the compressibility for *Rb. sphaeroides* is about twice as large as that for *Rps. acidophila* and *R. molischianum* and it was concluded that the packaging of the $\alpha\beta$-polypeptides is less tight in *Rb. sphaeroides*.

When looking at Fig. 2, the difference in spectral diffusion within the B800 band of LH2 from *Rsp. molischianum* with respect to that of *Rb. sphaeroides* and *Rps. acidophila* is striking. This can be already inferred from the widths of the histograms of the minor spectral changes, i.e., 1.7–4.5 $cm^{-1}$ for *Rb. sphaeroides* and *Rps. acidophila* versus 5–8.5 $cm^{-1}$ for *Rsp. molischianum*. This difference is even more obvious for the large spectral changes of ~250 $cm^{-1}$ that have been observed exclusively for *Rsp. molischianum*. The standard model for the description of the dynamics of materials like (bio-) polymers relies on the assumption that structural changes are supposed to only occur in spatially localized regions, which can be characterized by double well potentials. At low temperatures these potentials are approximated commonly as two-level systems (TLS) whose energies and tunneling matrix elements are randomly distributed (41). In previous work we have estimated the distance between the chromophore and those TLS that are associated with spectral changes of the order of some wavenumbers (29). Based on a dipole-dipole type interaction between the chromophore and the TLS we found a minimum distance of ~1 nm for the spectral changes that are in the order of a few wavenumbers and ~0.4 nm for those that are in the order of 10 $cm^{-1}$. Given the fact that the $Q_y$ electronic excitations of BChl *a* are mostly determined by the $\pi$-electron system in the bacteriochlorin plane it is reasonable to interpret these distances as the distance from this plane.

To link the spectral movements of the electronic transitions to conformational changes in the protein, it is interesting to compare the structural information that is available about the B800 binding pocket for the three species (21,22,42,43). In Fig. 5, the liganding of the B800 BChl *a* molecule is compared for *Rb. sphaeroides*, *Rsp. molischianum*, and *Rps. acidophila* from left to right. For *Rsp. molischianum* and *Rps. acidophila* this figure is based on the high-resolution x-ray structures (21,22) and for *Rb. sphaeroides* on a tentative model that will be discussed later. For better comparison the BChl *a* molecules are oriented with

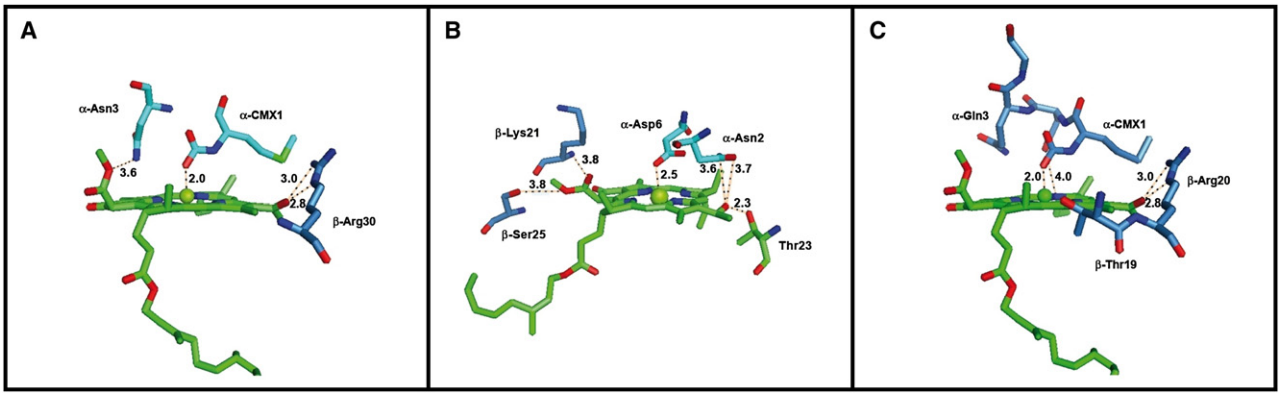


FIGURE 5 Part of the binding pocket for a B800 BChl *a* molecule in (*A*) *Rb. sphaeroides*, (*B*) *Rsp. molischianum*, and (*C*) *Rps. acidophila*. Dashed lines indicate likely hydrogen bonds and metal ligands at short distances given in Å.

their bacteriochlorin macrocycles parallel to the horizontal plane of the figure and have been rotated within this plane to have the connection between the macrocycle and the phytol chain in the same position.

The primary contact between the polypeptides of *Rps. acidophila* or *Rsp. molischianum* and the B800 molecules is between the central Mg ion and the residue that coordinates it. In the case of the LH2 complex from *Rps. acidophila*, the ligand is a carboxyl group attached to the initial αMet, Fig. 5 *C*. This ligation is supported by several hydrogen bonds, involving the surrounding residues $\alpha Asn^{2}$, $\alpha Gln^{3}$, and $\beta His^{12}$. Such a modification of the N-terminus of the α-apoprotein is not seen in the complex from *Rsp. molischianum*, where the $Mg^{2+}$ ion is coordinated by $\alpha Asp^{6}$. This ligation is supported by hydrogen bonds between $\alpha Asp^{6}$ and $\alpha Asn^{2}$, and a hydrogen bond between αAsp6 and a water molecule that also forms hydrogen bonds to one of the nitrogen atoms surrounding the Mg-ion on the BChl *a* molecule (Fig. 5 *B*). There is also a potential weak hydrogen bond between $\alpha Asn^{2}$ and one of the nitrogen atoms in the BChl *a* molecule. The overall binding pocket of *Rsp. molischianum* is more open and that has allowed the B800 molecule to rotate by 90° and tilt by 20° relative to the situation in the *Rps. acidophila* complex. However, in contrast to the B800 molecule in *Rps. acidophila*, where each B800 molecule only interacts within one αβ-heterodimer, the *Rsp. molischianum* B800 molecule interacts both within its own heterodimer and with the β-chain of the neighboring heterodimer (Fig. 5 *B*). The B800 molecule in *Rps. acidophila* reaches further in between the rings of transmembrane helices than in *Rsp. molischianum*. This may reduce the overall mobility of the bacteriochlorin ring in the case of *Rps. acidophila*. This is in line with what has been found for the crystallographic B factors for the B800 binding pocket for *Rps. acidophila* and *Rsp. molischianum,* which are displayed in Fig. 6 (22,44). The B factor (temperature factor) describes the displacement of atoms from their mean positions in the structure in the crystal, and can be used as an indirect measure of the mobility of groups of atoms. As represented in Fig. 6, the B factors from *Rps molischianum* are markedly higher across the BChl *a* molecule in the B800 binding pocket when compared to those for the BChl *a* molecule in the B800 binding pocket of *Rps. acidophila*. Although the B factors of LH2 from *Rps. molischianum* are higher across the whole of the protein, the internal differences between the B800 molecule and the protein itself are higher within the *Rps. molischianum* structure than within the structure from *Rps acidophila* (37 $Å^2$ and 57 $Å^2$ for *Rps. molischianum* protein and B800 molecule, respectively, and 20 $Å^2$ and 16 $Å^2$ for *Rps. acidophila* protein and B800 molecule, respectively). This observation agrees with the suggestion that the B800 molecule in *Rps. acidophila* has a reduced mobility compared with the one in *Rps. molischianum*.

In particular, very large B factors are observed for the phytol chain of BChl *a* in *Rsp. molischianum* suggesting that the protein in that part of the binding pocket allows the phytol chain to be mobile. Despite the nonpolar nature of the phytol chain this results in fluctuations of the local electric fields, which is usually taken into account by a multipole expansion and subsequent summation of the local contributions (45). Restricting ourselves to the leading term of such an expansion, i.e., the dipole-dipole interaction, and taking into account the estimates for the distances of the TLS that are involved in the minor spectral movements, it is likely that the increase in spectral diffusion between 1 to 10 $cm^{-1}$ for *Rsp. molischianum* is associated with the high mobility of the phytol chain for that species.

However, spectral changes in the order of 250 $cm^{-1}$, as observed for *Rsp. molischianum,* are so large that they probably reflect local conformational changes that affect the π-conjugation system of the bacteriochlorin macrocycle, e.g., by affecting the planarity of the ring, through a reorientation of side-groups, or through some rearrangement involving the central-Mg atom and its ligands (22,43, 46,47). This is corroborated when the surface charges of the residues in close proximity of the B800 BChl *a* π-conjugated electron system are compared for *Rsp. molischianum* and *Rps. acidophila* (Fig. 7) (48). In contrast to *Rps. acidophila*, where the protein environment in the vicinity of the bacteriochlorin ring is fairly neutral, the environment of this ring is negatively charged in the case of *Rsp. molischianum* giving rise to larger electrostatic interactions. Based on the accordance of the spectral diffusion statistics for *Rps. acidophila* and *Rb. sphaeroides*, i.e., the absence of very large spectral jumps in the order of 250 $cm^{-1}$, we conclude

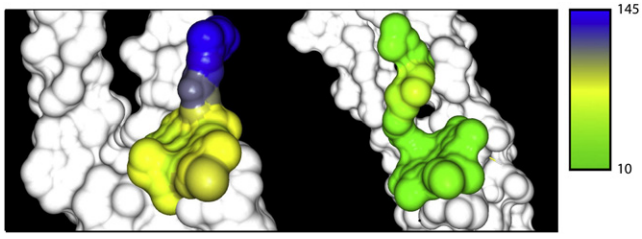


FIGURE 6 Crystallographic B-factors given in gray (color online) code for a space fill representation of the B800 BChl *a* molecule in *Rsp. molischianum* (*left*) and *Rps. acidophila* (*right*).

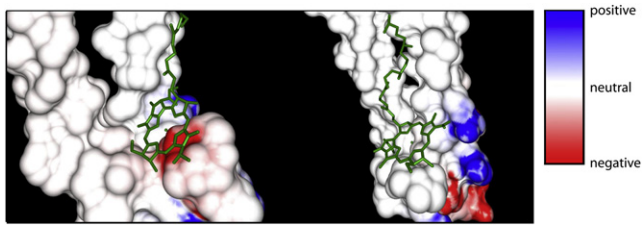


FIGURE 7 Surface charges in the B800 binding pocket in the vicinity of the bacteriochlorin plane of the BChl *a* molecule for *Rsp. molischianum* (*left*) and *Rps. acidophila* (*right*).

that the polarity of the B800 BChl *a* binding pocket is rather similar for these two species.

A tentative model for the B800 binding pocket in LH2 from *Rb. sphaeroides,* shown in Fig. 5 *A*, was created by threading the amino acid sequence through the structure of LH2 from *Rps. acidophila* (PDB code 1NKZ) using CHAINSAW from the CCP4 program suite (49,50). As the sequence identity is high, and the oligomeric state is thought to be the same, based on the results from electron microscopy, this was deemed to be a reasonable approach. As the protein sequence of the $\alpha$ apoprotein from *Rb. sphaeroides* has been shown to retain its N-terminal Met (51), our model contains a carboxylated Met as the coordinating residue of the Mg ion. As the residue in the *Rb. sphaeroides* sequence corresponding to $\alpha$Asn$^2$ in *Rps. acidophila* is a Thr this might cause the presence of one less hydrogen bond. However, because $\alpha$Gln$^3$ in the *Rps. acidophila* sequence is an Asn in the *Rb. sphaeroides* sequence, this may allow a new compensating hydrogen bond to be formed.

This work was supported by the Deutsche Forschungsgemeinschaft and the Biotechnology and Biological Sciences Research Council.

## REFERENCES


1. Nienhaus, G. U., and R. D. Young. 1996. Protein dynamics. *Encyclopedia Appl. Phys.* 15:163–184.
2. Frauenfelder, H., S. G. Sligar, and P. G. Wolynes. 1991. The energy landscapes and motions of proteins. *Science*. 254:1598–1603.
3. Frauenfelder, H., G. U. Nienhaus, and R. D. Young. 1994. Relaxation and disorder in proteins. *In* Disorder Effects on Relaxational Processes. R. Richert, editor. Springer-Verlag, Berlin. 591–614.
4. Fritsch, K., J. Friedrich, F. Parak, and J. L. Skinner. 1996. Spectral diffusion and the energy landscape of a protein. *Proc. Natl. Acad. Sci. USA*. 93:15141–15145.
5. Oikawa, H., S. Fujiyoshi, T. Dewa, M. Nango, and M. Matsushita. 2008. How deep is the potential well confining a protein in a specific conformation? A single-molecule study on temperature dependence of conformational change between 5 and 18 K. *J. Am. Chem. Soc.* 130: 4580–4581.
6. Hofmann, C., T. J. Aartsma, H. Michel, and J. Köhler. 2003. Direct observation of tiers in the energy landscape of a chromoprotein: a single-molecule study. *Proc. Natl. Acad. Sci. USA*. 100:15534–15538.
7. Hofmann, C., T. J. Aartsma, H. Michel, and J. Köhler. 2004. Spectral dynamics in the B800 band of LH2 from *Rhodospirillum molischianum*: a single-molecule study. *N. J. Phys.* 6:1–15.
8. Rätsep, M., J. Linnanto, and A. Freiberg. 2009. Mirror symmetry and vibrational structure in optical spectra of chlorophyll a. *J. Chem. Phys.* 130:194501.
9. Rebane, K. K. 1970. Impurity Spectra of Solids. Plenum Press, New York.
10. Keil, T. H. 1965. Shapes of impurity absorption bands in solids. *Phys. Rev.* 140:601–617.
11. Berlin, Y., A. Burin, J. Friedrich, and J. Köhler. 2006. Spectroscopy of proteins at low temperature. Part I: experiments with molecular ensembles. *Phys. Life Rev.* 3:262–292.
12. Renge, I. 1992. Relationship between electron-phonon coupling and intermolecular interaction parameters in dye-doped organic glasses. *J. Opt. Soc. Am. B.* 9:719–723.
13. Rätsep, M., R. E. Blankenship, and G. J. Small. 1999. Energy transfer and spectral dynamics of the three lowest energy $Q_y$ states of the Fenna-Matthews-Olson antenna complex. *J. Phys. Chem. B.* 103:5736–5741.
14. Creemers, T. M. H., C. de Caro, R. W. Visschers, R. van Grondelle, and S. Völker. 1999. Spectral hole burning and fluorescence line narrowing in subunits of the light harvesting complex LH1 of purple bacteria. *J. Phys. Chem. B.* 103:9770–9776.
15. Schlichter, J., J. Friedrich, M. Parbel, and H. Scherr. 2001. New concepts in spectral diffusion physics of proteins. *Phot. Sci. News.* 6:100–110.
16. Skinner, J. L., J. Friedrich, and J. Schlichter. 1999. Spectral diffusion in proteins. *J. Phys. Chem. A.* 103:2310–2311.
17. Ambrose, W. P., Th Basché, and W. E. Moerner. 1991. Detection and spectroscopy of single pentacene molecules in a *p*-terphenyl crystal by means of fluorescence excitation. *J. Chem. Phys.* 95:7150–7163.
18. Jang, S., and R. J. Silbey. 2003. Theory of single molecule line shapes of multichromophoric macromolecules. *J. Chem. Phys.* 118:9312–9323.
19. Hofmann, C., H. Michel, M. van Heel, and J. Köhler. 2005. Multivariate analysis of single-molecule spectra: Surpassing spectral diffusion. *Phys. Rev. Lett.* 94:195501.
20. Hildner, R., U. Lemmer, U. Scherf, M. van Heel, and J. Köhler. 2007. Revealing the electron-phonon coupling in a conjugated polymer by single-molecule spectroscopy. *Adv. Mater.* 19:1978–1982.
21. McDermott, G., S. M. Prince, A. A. Freer, A. M. Hawthornthwaite-Lawless, M. Z. Papiz, et al. 1995. Crystal structure of an integral membrane light-harvesting complex from photosynthetic bacteria. *Nature*. 374:517–521.
22. Koepke, J., X. Hu, C. Muenke, K. Schulten, and H. Michel. 1996. The crystal structure of the light harvesting complex II (B800–B850) from *Rhodospirillum molischianum*. *Structure*. 4:581–597.
23. Walz, T., S. J. Jamieson, C. M. Bowers, P. A. Bullough, and C. N. Hunter. 1998. Projection structures of three photosynthetic complexes from *Rhodobacter sphaeroides*: LH2 at 6 angstrom LH1 and RC-LH1 at 25 angstrom. *J. Mol. Biol.* 282:833–845.
24. Hu, X., T. Ritz, A. Damjanovic, F. Autenrieth, and K. Schulten. 2002. Photosynthetic apparatus of purple bacteria. *Q. Rev. Biophys.* 35:1–62.
25. Cogdell, R. J., A. Gall, and J. Köhler. 2006. The architecture and function of purple bacteria: from single molecules to in vivo membranes. *Q. Rev. Biophys.* 39:227–324.
26. Hofmann, C., F. Kulzer, R. Zondervan, J. Köhler, and M. Orrit. 2008. Single biomolecules at cryogenic temperatures: from structure to dynamics. *In* Biophysics: Single Molecules and Nanotechnology, Vol. 12. R. Rigler and H. Vogel, editors. Springer-Verlag, Berlin, Heidelberg, pp. 25–51.
27. Monshouwer, R., M. Abrahamson, F. van Mourik, and R. van Grondelle. 1997. Superradiance and exciton delocalization in bacterial photosynthetic light-harvesting systems. *J. Phys. Chem. B.* 101:7241–7248.
28. Baier, J., M. F. Richter, R. J. Cogdell, S. Oellerich, and J. Köhler. 2007. Do proteins at low temperature behave as glasses? A single-molecule study. *J. Phys. Chem. B.* 111:1135–1138.
29. Baier, J., M. F. Richter, R. J. Cogdell, S. Oellerich, and J. Köhler. 2008. Determination of the spectral diffusion kernel of a protein by single molecule spectroscopy. *Phys. Rev. Lett.* 100:018108.
30. Hofmann, C., M. Ketelaars, M. Matsushita, H. Michel, T. J. Aartsma, et al. 2003. Single-molecule study of the electronic couplings in a circular array of molecules: light-harvesting-2 complex from *Rhodospirillum molischianum*. *Phys. Rev. Lett.* 90:013004.
31. Evans, M. B., A. M. Hawthornthwaite, and R. J. Cogdell. 1990. Isolation and characterization of the different B800–850 light-harvesting complexes from low- and high-light grown cells of *Rhodopseudomonas palustris*, strain 2.1.6. *Biochim. Biophys. Acta*. 1016:71–76.
32. Richter, M. F., J. Baier, R. J. Cogdell, J. Köhler, and S. Oellerich. 2007. Single-molecule spectroscopic characterization of light-harvesting 2 complexes reconstituted into model membranes. *Biophys. J.* 93:183–191.

33. Lang, E., J. Baier, and J. Köhler. 2006. Epifluorescence, confocal and total internal reflection microscopy for single-molecule experiments: a quantitative comparison. *J. Microsc.* 222:118–123.

34. van Heel, M., B. Gowen, R. Matadeen, E. V. Orlova, R. Finn, et al. 2000. Single-particle electron cryo-microscopy: towards atomic resolution. *Q. Rev. Biophys.* 33:307–369.

35. van Heel, M. 1991. A new family of powerful multivariate statistical sequence analysis techniques. *J. Mol. Biol.* 220:877–887.

36. Orrit, M., J. Bernard, R. Brown, and B. Lounis. 1996. Optical spectroscopy of single molecules in solids. *In* Progress in Optics. E. Wolf, editor. Elsevier, Amsterdam. 61–144.

37. de Caro, C., R. W. Visschers, R. van Grondelle, and S. Völker. 1994. Inter- and intraband energy transfer in LH2 antenna complexes of purple bacteria. A fluorescence line narrowing and hole-burning study. *J. Phys. Chem.* 98:10584–10590.

38. van Oijen, A. M., M. Ketelaars, J. Köhler, T. J. Aartsma, and J. Schmidt. 2000. Spectroscopy of individual LH2 complexes of *Rhodopseudomonas acidophila*: diagonal disorder, sample heterogeneity, spectral diffusion, and energy transfer in the B800 band. *Biophys. J.* 78:1570–1577.

39. Limantara, L., S. Sakamoto, Y. Koyama, and H. Nagae. 1997. Effects of nonpolar and polar solvents on the $Q_x$ and $Q_y$ energies of bacteriochlorophyll a and bacteriopheophytin *a*. *Photochem. Photobiol.* 65: 330–337.

40. Wu, H.-M., M. Rätsep, R. Jankowiak, R. J. Cogdell, and G. J. Small. 1997. Comparison of the LH2 antenna complex of *Rhodopseudomonas acidophila* (strain 10050) and *Rhodobacter sphaeroides* by high pressure absorption, high pressure hole burning, and temperature dependent absorption spectroscopies. *J. Phys. Chem. B.* 101:7641–7653.

41. Anderson, P. W., B. I. Halperin, and C. M. Varma. 1972. Anomalous low-temperature thermal properties of glasses and spin glasses. *Philos. Mag.* 25:1–9.

42. Cogdell, R. J., N. W. Isaacs, A. A. Freer, T. D. Howard, A. T. Gardiner, et al. 2003. The structural basis of light-harvesting in purple bacteria. *FEBS Lett.* 555:35–39.

43. He, Z., V. Sundström, and T. Pullerits. 2002. Influence of the protein binding site on the excited states of bacteriochlorophyll: DFT calculations of B800 in LH2. *J. Phys. Chem. B.* 106:11606–11612.

44. Papiz, M. Z., S. M. Prince, T. Howard, R. J. Cogdell, and N. W. Isaacs. 2003. The structure and thermal motion of the B800-850 LH2 complex from *Rps. acidophila* at 2.0 (Å)over-circle resolution and 100 K: new structural features and functionally relevant motions. *J. Mol. Biol.* 326:1523–1538.

45. Madjet, M. E., A. Abdurahman, and T. Renger. 2006. Intermolecular coulomb couplings from ab initio electrostatic potentials: application to optical transitions of strongly coupled pigments in photosynthetic antennae and reaction centers. *J. Chem. Phys. B.* 110:17268–17281.

46. Gudowska-Nowak, E., M. D. Newton, and J. Fajer. 1990. Conformational and environmental effects on bacteriochlorophyll optical spectra: correlations of calculated spectra with structural results. *J. Phys. Chem.* 94:5795–5801.

47. Germeroth, L., F. Lottspeich, B. Robert, and H. Michel. 1993. Unexpected similarities of the B800–850 light harvesting complex from *Rhodospirillum molischianum* to the B870 light-harvesting complexes from other photosynthetic bacteria. *Biochemistry.* 32:5615–5621.

48. Petrey, D., and B. Honig. 2003. GRASP2: visualization, surface properties, and electrostatics of macromolecular structures and sequences. *Methods Enzymol.* 374:492–509.

49. Stein, N. 2008. CHAINSAW: a program for mutating pdb files used as templates in molecular replacement. *J. Appl. Cryst.* 41:641–643.

50. Collaborative Computational Project, Number 4. 1994. The CCP4 suite: programs for protein crystallography. *Acta Crystallogr D Biol Crystallogr.* 50:760–763.

51. Theiler, R., F. Suter, H. Zuber, and R. J. Cogdell. 1984. A Comparison of the primary structures of the two B800-850-apoproteins from wild-type *Rhodobacter sphaeroides* strain 2.4.1 and a carotenoidless mutant strain R26.1. *FEBS Lett.* 175:231–237.